Assessment of Two-Temperature Kinetic Model for Ionizing Air

Chul Park*
NASA Ames Research Center, Moffett Field, California

A two-temperature chemical-kinetic model for air is assessed by comparing theoretical results with existing experimental data obtained in shock tubes, ballistic ranges, and flight experiments. In the model, one temperature (T) is assumed to characterize the heavy-particle translational and molecular rotational energies, and another temperature (T_v) the molecular vibrational, electron translational, and electronic excitation energies. The theoretical results for nonequilibrium flow in shock tubes are obtained using the computer code STRAP (shock-tube radiation program) and for flow along the stagnation streamline in the shock layer over spherical bodies using the newly developed code SPRAP (stagnation-point radiation program). Substantial agreement is shown between the theoretical and experimental results for relaxation times and radiative heat fluxes. At very high temperatures, the spectral calculations need further improvement. The present agreement provides strong evidence that the two-temperature model characterizes principal features of nonequilibrium airflow. New theoretical results using the model are presented for the radiative heat fluxes at the stagnation point of 6 m radius sphere, representing an aeroassisted orbital transfer vehicle, over a range of freestream conditions. Assumptions, approximations, and limitations of the model are discussed.

Nomenclature

c = average molecular speed $\sqrt{8kT/\pi m}$, cm s^{-1}
C = pre-exponential factor in reaction rate coefficient, cm^{3}mole^{-1}s^{-1}
e_v = average vibrational energy per particle, erg
e_{ve} = average vibrational energy per particle under equilibrium, erg
E = reaction energy, erg
k = Boltzmann constant, 1.3805×10^{-16} erg K^{-1}
m = mass of a particle, g
M = unspecified colliding partner in chemical reaction
n = temperature exponent on reaction-rate coefficient
N = number density, cm^{-3}
P_∞ = freestream pressure, atm
q_r = radiative heat flux at the stagnation point, W cm^{-2}
q_{ne} = radiative heat flux integrated from the shock wave to $x = x_e$, W cm^{-2}
R = nose radius, m
T = heavy-particle translational-rotational temperature, K
T_a = geometrically averaged temperature $\sqrt{TT_v}$
T_s = translation-rotational temperature behind the normal shock, K
T_v = vibrational-electron translational-electronic temperature, K
T_{vs} = vibrational-electron translational-electronic temperature behind normal shock, K
x = distance behind normal shock, cm
x_e = distance measured from the foot of luminosity profile to the point where luminosity is 1.1 times the equilibrium (plateau) value, cm
x_p = distance measured from the foot of luminosity profile to the point where luminosity peaks
V_∞ = freestream velocity, km/s
ρ_0 = standard density at sea level, 1.29 kg m^{-3}
ρ_∞ = freestream density, kg m^{-3}
σ_v = cross section for vibrational relaxation at infinitely large temperature, cm^2
τ = total relaxation time for vibrational excitation, s
τ_c = relaxation time for vibrational excitation given by the collision theory at high temperatures, s
τ_e = time measured from the foot of luminosity profile to the point where luminosity is 1.1 times the equilibrium (plateau) value, s
τ_L = relaxation time for vibrational excitation determined by Landau–Teller theory as computed using the correlation formula of Millikan and White, s
τ_p = time measured from the foot of luminosity profile to the point where luminosity peaks, s

Introduction

THE problems of chemical nonequilibrium in the shock layers over the vehicles flying at high speeds and high altitudes in the Earth's atmosphere have been discussed by several investigators.[1-4] Most of the existing computer codes for calculating the nonequilibrium reacting flow use the one-temperature model, which assumes that all of the internal energy modes of the gaseous species are in equilibrium with the translational mode.[3,4] It has been pointed out that such a one-temperature description of the flow leads to a substantial overestimation of the rate of equilibration when compared with the existing experimental data.[2] A three-temperature chemical-kinetic model has been proposed by Lee[5] to describe the relaxation phenomena correctly in such a flight regime. However, the model is quite complex and requires many chemical rate parameters that are not yet known. As a compromise between the three-temperature chemical-kinetic and the conventional one-temperature model, a two-temperature chemical-kinetic model has been developed.[6,7] The model uses one temperature T to characterize the translational energy of the atoms and molecules and the rotational energy of the molecules, and another temperature T_v to characterize the vibrational energy of the molecules, translational energy of the electrons, and electronic excitation energy of atoms and molecules. The model has been applied to compute the thermodynamic properties behind a normal shock wave in a flow through a constant-area duct.[6,7] Radiation emission from the

Presented as Paper 87-1547 at the AIAA 22nd Thermophysics Conference, Honolulu, HI, June 8–10; received Aug. 3, 1987; revision received May 6, 1988. This paper is declared a work of the U.S. Government and therefore is not subject to copyright protection in the United States.

*Research Scientist. Associate Fellow AIAA.

nonequilibrium flow has been calculated using the nonequilibrium air radiation (NEQAIR) program.[8,9] The flow and the radiation computations have been packaged into a single computer program, named the shock-tube radiation program (STRAP).[7]

A first-step assessment of the two-temperature model was made in Ref. 7 where it was used in computing flow properties and radiation emission from the flow in a shock tube for pure nitrogen undergoing dissociation and weak ionization (ionization fraction less than 0.1%). Generally good agreement was found between the calculated radiation emission and those obtained experimentally in shock tubes.[10–12] The only exception involved the vibrational temperature. The theoretical treatment of the vibrational temperature could not be validated because the existing data on the vibrational temperature behind a normal shock wave[12] are those for an electronically excited state of the molecular nitrogen ion N_2^+ instead of the ground electronic state of the neutral nitrogen molecule N_2 that is calculated in the theoretical model. The measured vibration temperature of N_2^+ was much smaller than the calculated vibrational temperature for N_2.

The purpose of the present work is to extend the assessment of the two-temperature model by using it to predict the radiation emissions in air previously measured under a wide range of experimental conditions where the ionization fraction is of the order of 1%. The theoretical values are calculated for a freestream gas mixture of 21% O_2 and 79% N_2 to approximate the composition of air, and the 11 species, N, O, N_2, O_2, NO, N^+, O^+, N_2^+, O_2^+, NO^+, and e^-, are considered in describing the chemical composition of the ionized mixture. The experimental data used in the assessment were obtained from laboratory and flight experiments reported in the literature. The laboratory data were taken in both shock-tubes[13–15] and ballistic ranges,[16,17] and the flight data were taken on the Project Fire[18] and Planetary Atmosphere Experiment Test (PAET)[19,20] experiments. The calculated results are compared with all these data and, as will be shown, the current model reproduces the experimental data remarkably well.

New estimates using the current two-temperature model are presented for the radiative heat fluxes at the stagnation point of a sphere of 6-m radius in a freestream flow consisting of the 21% O_2-79%N_2 mixture over a range of freestream velocities and densities. The chosen conditions are representative of the size and flight conditions for the proposed Aeroassisted Orbital Transfer Vehicle (AOTV). Finally, the limitations of the model are discussed.

Method of Calculation

The present two-temperature thermochemical model is identical to that in Ref. 7. The model assumes that the rotational temperature is the same as the translational temperature of the heavy particles and is denoted by T. This assumption is based on the knowledge that the energy exchange between the translational and rotational modes is very fast. The model assumes that the average rotational energy content of a molecule is kT, where k is the Boltzmann constant, in accordance with the classical theory of a rigid rotator.

The model assumes also that the vibrational temperature of the molecules, translational temperature of the electrons, and electronic excitation temperature of the atoms and molecules are the same in the computation of the flow properties and are denoted by T_v. The assumption that these three temperatures are the same is based on the knowledge that the energy transfer between the translational motion of the free electrons and the vibrational motion of N_2 molecule is very fast,[5,21] and that the low-lying electronic states of atoms and atoms and molecules, which contain most of the electronic excitation energies of the mixture, equilibrate quickly with the ground electronic state with populations appropriate to the electron temperature.[5] The average vibrational energy per molecule e_v is expressed using the classical harmonic oscillator model, that is, by kT_v. Electronic excitation energy is calculated under the assumption that there is no coupling among the rotational, vibrational, and electronic modes in a molecule. This last assumption holds approximately true for temperatures up to about 10,000 K with an error of about 1% and up to about 15,000 K with an error of about 10%.

The assumption that the electronic excitation temperature is the same as the vibrational and electron temperatures is removed later in the computation of nonequilibrium radiation using the program NEQAIR.[8,9] Within NEQAIR, the populations of the electronically excited states of atoms and molecules are calculated by solving the conservation equations for the states.[8]

The conservation equation for the vibrational-electron-electronic temperature T_v accounts for 1) vibrational excitation by collisions with heavy particles, 2) elastic energy exchange between electron and heavy-particle gases, 3) removal of electron translational energy by electron-impact ionization and electron-impact dissociation, and 4) gains and losses of electronic excitation energies during dissociation. The method does not account for the preferential removal of highly vibrational states in dissociation.[22] However, the phenomenon is implicitly incorporated because the experimental rate coefficient values used for the calculation account for the effect, as the rate coefficients have been deduced using the one-temperature model.

The rate coefficients used in the calculation are listed in Table 1. The sources of the rate parameters are given in the Appendix. As stated in Table 1, the rate coefficients for thermal dissociation are assumed to be dictated by the geometric average temperature $T_a = \sqrt{TT_v}$. Note that a large rate constant ($C = 8.3 \times 10^{24}$) is used for the electron-impact dissociation rate of N_2. This coefficient and other coefficients involving nitrogen are identical to those used in Ref. 7.

The vibrational relaxation rate is calculated using the modified form of the correlation formula of Millikan and White.[23] The modification accounts for two phenomena that are unique to the high-temperature environment, that is, a limiting value of the cross section and the diffusive nature of vibrational relaxation. The first phenomenon arises from the fact that the correlation formula of Millikan and White implies an unrealistically large cross section for vibrational relaxation at high temperatures. Reference 2 devised a correction procedure for this phenomenon by introducing a limiting cross section σ_v. According to the procedure, the effective relaxation time τ is taken to be the sum of Millikan and White's value τ_L and the value determined from σ_v

$$\tau = \tau_L + \tau_c \tag{1}$$

where

$$\tau_c = 1/(c\sigma_v N)$$

and c is the average molecular speed $c = \sqrt{8kt/\pi m}$ and N the number density of the colliding particles. The numerical value of σ_v is currently unknown and is adjusted to satisfy existing experimental data. In Ref. 7, the most appropriate value of σ_v for nitrogen at temperatures below 19,000 K was found to be 10^{-16} cm^2. In the present work, the temperature range of concern varies up to 62,000 K. For this wider temperature range, the most appropriate value of σ_v was found to be

$$\sigma_v = 10^{-17}(50{,}000/T)^2 \tag{2}$$

This new σ_v value reproduces the nitrogen data considered in Ref. 7 and the air data in the present work, as will be shown later.

The second correction for the vibrational relaxation just mentioned accounts for the fact that, at high temperatures, vibrational relaxation obeys a diffusion equation with respect to the vibrational energy levels, rather than a Landau–Teller-type rate equation.[5,21,24] As a result, the vibrational relaxation

Table 1 Reaction rate parameters C, n, and E/k and controlling temperature T_x in the forward-rate coefficient expression $k_f = CT_x^n \exp(-E/kT_x)$, where C is in $cm^3 mole^{-1} s^{-1}$

Reaction	T_x	M	C	n	E/k
$O_2 + M \rightarrow O + O + M$	$\sqrt{TT_v}$	N	2.90^{23}	−2.0	59,750
		O	2.90^{23}	−2.0	59,750
		N_2	9.68^{22}	−2.0	59,750
		O_2	9.68^{22}	−2.0	59,750
		NO	9.68^{22}	−2.0	59,750
		e^-	9.68^{22}	−2.0	59,750
$N_2 + M \rightarrow N + N + M$	$\sqrt{TT_v}$	N	1.60^{22}	−1.6	113,200
		O	4.98^{22}	−1.6	113,200
		N_2	3.70^{21}	−1.6	113,200
		O_2	3.70^{21}	−1.6	113,200
		NO	4.98^{21}	−1.6	113,200
		e^-	8.30^{24}	−1.6	113,200
$NO + M \rightarrow N + O + M$	$\sqrt{TT_v}$	N	7.95^{23}	−2.0	75,500
		O	7.95^{23}	−2.0	75,500
		N_2	7.95^{23}	−2.0	75,500
		O_2	7.95^{23}	−2.0	75,500
		NO	7.95^{23}	−2.0	75,500
		e^-	7.95^{23}	−2.0	75,500
$NO + O \rightarrow N + O_2$	T		8.37^{12}	0	19,450
$O + N_2 \rightarrow N + NO$	T		6.44^{17}	−1.0	38,370
$O - O_2^+ \rightarrow O_2 + O^+$	T		6.85^{13}	−0.52	18,600
$N_2 + N^+ \rightarrow N + N_2^+$	T		9.85^{12}	−0.18	12,100
$O + NO^+ \rightarrow NO + O^+$	T		2.75^{13}	0.01	51,000
$N_2 + O^+ \rightarrow O + N_2^+$	T		6.33^{13}	−0.21	22,200
$O_2 + NO^+ \rightarrow NO + O_2^+$	T		1.03^{16}	−0.17	32,400
$NO^+ + N \rightarrow N_2^+ + O$	T		1.70^{13}	0.40	35,500
$O + N \rightarrow NO^+ + e^-$	T		1.53^{9}	0.37	3200
$O + O \rightarrow O_2^+ + e^-$	T		3.85^{9}	0.49	80,600
$N + N \rightarrow N_2^+ + e^-$	T		1.79^{9}	0.77	67,500
$O + e^- \rightarrow O^+ + e^- + e^-$	T_v	e^-	3.90^{33}	−3.90	158,500
$N + e^- \rightarrow N^+ + e^- + e^-$	T_v	e^-	2.50^{34}	−3.82	168,600

rate does not vary linearly with the difference in vibrational energies $(e_{ve} - e_e)$ as given by the Landau–Teller equation, but is proportional to its sth power, where s is larger than unity, in the form[5,7,21]

$$\frac{\partial e_v}{\partial t} = \frac{e_{ve} - e_v}{\tau} \left| \frac{T_s - T_v}{T_s - T_{vs}} \right|^{s-1} \tag{3}$$

Reference 21 shows that in the high-temperature limit, s should approach 3.5. In Ref. 7, a bridging formula is proposed in the form

$$s = 3.5 \exp(-5000/T_s) \tag{4}$$

where T_s is the translational-rotational temperature immediately behind the normal shock wave. This formula is adopted in the present work.

The computer program STRAP, mentioned earlier, contains the kinetic model just described. With this model, the program calculates the flow through a constant-area tube by solving fluid-mechanical conservation equations. The program assumes the flow to be viscous. The transport properties necessary for the viscous flow calculation are determined using the cross-section data of Yos.[25] The program uses an implicit time-marching technique with spatial central-differencing without added artificial viscosity and relies on physical viscosity for convergence. As a result, the method converges only when the flow Reynolds number (defined by the length of the computing domain and velocity, density, and viscosity immediately behind the normal shock) is below about 10,000. Thus, the viscous calculation is done only over the short distance for which the Reynolds number is small. For the region beyond this point, an inviscid flow was assumed. The computation of chemical reactions in the inviscid region is an initial value problem involving only ordinary differential equations. A standard library subroutine was used for integrating these equations.

Comparing the current calculation with the data obtained in a shock tube requires a slight adjustment to the density and temperatures determined by the foregoing procedure. The density and temperatures are multiplied by the factors $(1 + 0.025x)$ and $(1 + 0.01x)$, where x is the distance from the shock wave in centimeters, to account for the boundary-layer growth on the wall of the shock tube,[7] as the boundary layer tends to compress the test gas adiabatically. Existing shock-tube data (e.g., Ref. 26) indicate that the compression occurs approximately linearly with distance over a small range of x, and the linear form of the multiplicative factors chosen expresses this relationship. The numerical values of the coefficients are chosen to reproduce the radiation characteristics observed in the shock-tube experiments at large x where the flow is believed to be in equilibrium, and therefore any rise in radiation intensity is attributable to the compression phenomenon. The ratio of the two coefficients (0.025 and 0.010) is consistent with an adiabatic compression with an effective specific heat ratio of 1.4.

The calculation of the nonequilibrium radiation was done using the code NEQAIR,[8,9] that was incorporated into STRAP. This code requires the nonequilibrium thermodynamic properties as inputs and calculates the number densities of various electronic states by invoking the so-called quasi-steady-state condition for the conservation of the individual electronic states. The quasi-steady-state condition is based on the assumption that the rates for populating and depopulating any electronic state are both much faster than the difference between them, which is the rate of change of the state population. The rates for populating and depopulating any state are given by the collisional and radiative transition rates. This assumption is believed to be valid in most of the continuum flow regimes considered in the present work.

The transition probabilities and molecular radiation intensity factors used in the present work are identical to those used in Refs. 2, 7, and 8.

The theoretical spectral results incorporated the effect of instrumental broadening to compare with the experimental data taken in a shock tube.[13] In the shock-tube experiment,[13] radiation was observed through a slit of 0.5 mm. To account for this effect, the calculated radiation intensity is folded[27] by a Gaussian slit of 0.5 mm width at half-height. Also, radiation at wavelengths below 0.2 μm is assumed to be totally absorbed and hence, is not calculated. Radiation at wavelengths longer than 0.2 μm is assumed to be optically thin. The maximum wavelength considered was 1.5 μm.

The flow properties along the stagnation streamline in the flow over a spherical blunt body were calculated by using the assumption that the flow properties are a function only of the flow residence time, that is, the time elapsed since the flow passed through the shock wave. Thus, the properties at a point on the stagnation streamline are assumed to be the same as those at the point behind a normal shock where the flow residence time is the same, as illustrated schematically in Fig. 1. For the points within the boundary layer, the properties so determined are further modified to account for cooling and diffusion effects. For this region, T, T_v, and the mole fractions of the ions are assumed to vary linearly with a normalized energy function g that is defined as g = (local enthalpy)/(post-shock enthalpy). This assumption forces the ions to be neutralized completely at the surface. That is, the wall surface is totally catalytic to ionic recombination, but noncatalytic to atomic recombination (catalytic efficiency less than about 0.1). Such an assumption is approximately true if the wall is made of a metallic oxide. A metallic oxide is an electric insulator that requires equality between electron and ion fluxes, which can be satisfied only by full ionic recombination. Furthermore, a metallic oxide tends to be noncatalytic to atomic recombination. In the Project Fire and PAET experiments concerned in the present work, the wall was made of a metal, which most likely would have produced a thin metal oxide on its outermost layer.

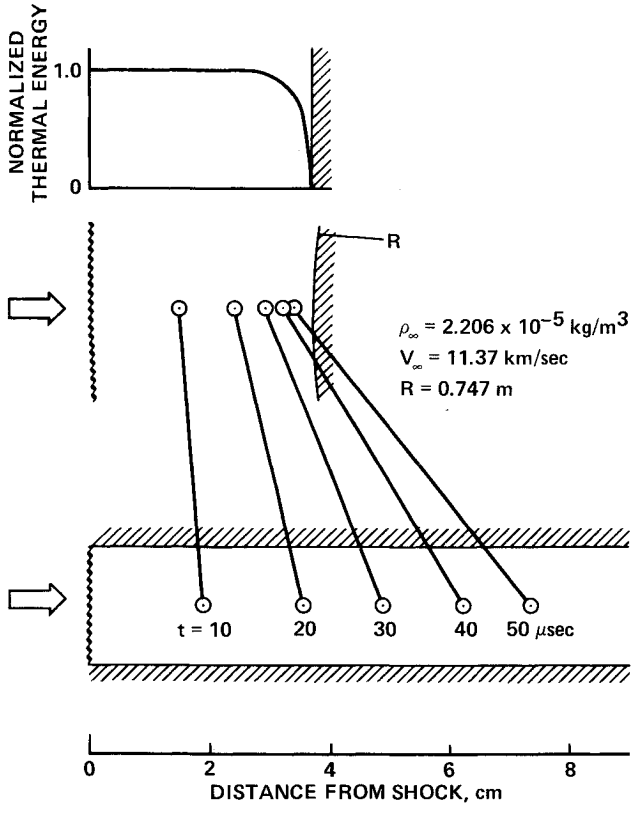

Fig. 1 Schematic showing the correspondence between the flow along the stagnation streamline and the flow through a constant-area tube. The case shown is for Fire 2 vehicle at 79.1 km altitude.

The flow residence times and normalized energy function g needed in these calculations are obtained by solving the viscous-shock-layer equation[28] for the stagnation region assuming a constant Prandtl number of 0.7. The solutions to the viscous-shock-layer calculation are obtained by iteration. First, a density profile is assumed to be the same as that in a constant-area tube. By integrating the viscous-shock-layer equations in the stagnation region using these first-guess density values, one obtains velocity and energy profiles. The velocity profile provides improved residence time estimates, and the energy profile is used to modify T, T_v, and ion concentrations. From these, an improved estimate of the density distribution is obtained and the next-step iteration is carried out. This viscous-shock-layer calculation is packaged into a program named SPRAP (stagnation-point radiation program). An earlier version of this program has been used in calculating the radiative heat fluxes at the stagnation point of a sphere in Ref. 29. However, the iterative procedure used in the earlier version did not produce well-converged solutions. Fairly substantial differences in calculated radiative heat fluxes are found between the earlier and current version of this program.

Comparison with Experiments

Shock-Tube Data

The heavy-particle translational-rotational temperature T, vibrational-electron-electronic temperature T_v, and total emission intensity are shown in Fig. 2 for the flow in a shock tube at an initial driven-section pressure of 0.1 Torr and shock velocity of 10 km/s. As seen here, T, is initially about 49,000 K behind the shock wave and decreases monotonically, whereas T_v is initially about 1700 K behind the shock and reaches 11,600 K at its peak. The emission intensity is zero at $x = 0$, starts to rise at $x = 0.2$ cm, and reaches a peak value of 33 W/cm^3 at $x = 0.5$ cm. The inset in the lower part of the figure shows the oscillograph record of the intensities of two prominent spectral features obtained experimentally under the same conditions.[13] The radiation at wavelengths between 0.40 and 0.42 μm comprises mostly that of the first negative band

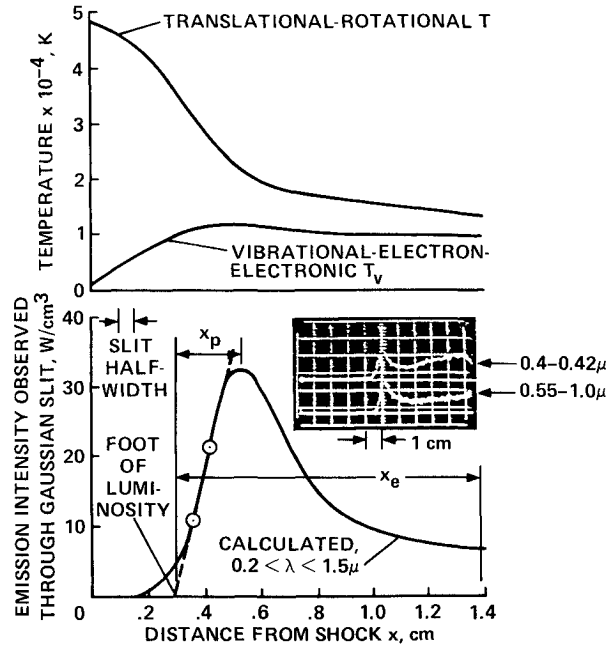

Fig. 2 Calculated temperatures T and T_v and radiation emission behind shock; $p_\infty = 0.1$ Torr, $V_\infty = 10$ km/s. The inset shows the oscillograph records of radiation at wavelength ranges 0.40 to 0.42 and 0.55 to 1.0 μm obtained by Allen et al.[13]

system of N_2^+, and that in the wavelength range from 0.55 to 1.0 μm contains line radiation from N and O atoms and the first positive system of N_2. As seen here, the calculated profile resembles the experimental profiles reasonably well up to $x = 1.4$ cm. The two radiation intensities reach a peak approximately at the same location even though their radiation mechanisms are not directly related. Although not shown in the figure, the present calculation also illustrates that the peaks of the radiation intensities from the two wavelength regions occur approximately at the same location. At $x =$ 2 cm, the experimental luminosity reaches a plateau, which is interpreted in Ref. 16 to be the equilibrium region. Beyond 2 cm, the experimental intensity rises. This rise is attributable to the compression caused by the growth of the boundary layer over the shock-tube wall mentioned earlier. Although not shown here, this rise is reproduced approximately in the present calculation by virtue of the multiplicative factors of $(1 + 0.025x)$ for density and $(1 + 0.01x)$ for temperatures.

The location of the normal shock is not known exactly in the shock-tube experiment.[13] The curvature of the shock prevented exact determination of the shock position. Therefore, in the experiment, the relaxation distances were determined from the intensity record for the red wavelength region (0.55 to 1.0 μm) alone. The "foot" of luminosity was first determined by drawing a straight line through the rising portion of the intensity profile and finding its intersection with the horizontal axis. The same procedure is followed in determining the foot of luminosity in the present theoretical work. That is, a straight line is drawn between the one-third and two-thirds points on the rising portion of the curve to determine the intersection, as shown in Fig. 2. The distance to the peak radiation point x_p is measured from the foot of luminosity found in this way. The corresponding time τ_p is determined by dividing x_p by the flow velocity. The equilibration point is defined in the shock-tube experiment[13] as the point where the intensity of the red radiation becomes 1.1 times the equilibrium value. The same criterion is used for the theoretical results. The equilibration distance x_e and corresponding time τ_e are also determined from the foot of luminosity.

The thermodynamic conditions at the peak intensity point and equilibration point are listed in Table 2. Here, T and T_v are 21,900 and 11,600 K at the peak intensity point. The peak intensity point occurs during the broad peak in T_v, thereby suggesting that it is mostly T_v, which represents the electronic excitation temperature and radiation intensity. The species concentrations for the case shown in Fig. 2 are shown in Fig.

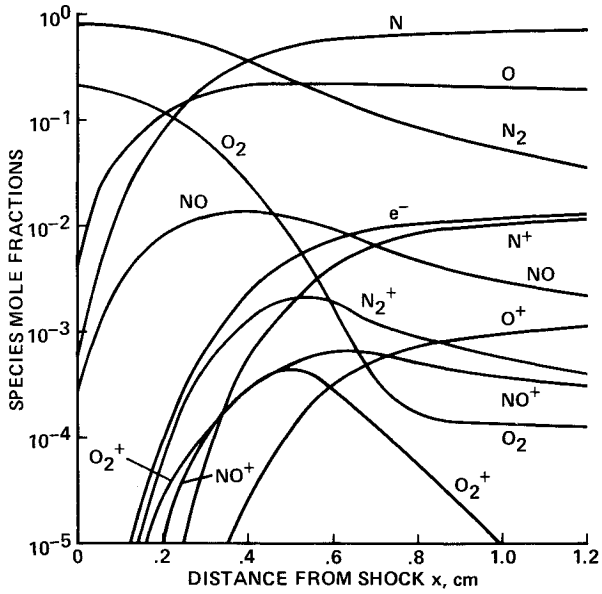

Fig. 3 Calculated species mole fractions; $p_\infty = 0.1$ Torr, $V_\infty =$ 10 km/s.

Table 2 Typical shock-tube test conditions

Freestream conditions	
Temperature T_∞	300 K
Pressure p_∞	0.1 Torr
Density ρ_∞	1.612×10^{-7} g/cm^3
Shock velocity V_∞	10 km/s
Peak radiation point conditions	
Location measured from shock	0.526 cm
Location measured from foot of luminosity x_p	0.240 cm
Time measured from foot of luminosity τ_p	0.240 μs
$\tau_p p_\infty$	3.28×10^{-5} μs-atm
T	21,933 K
T_v	11,618 K
Species mole fractions	
N	0.5308
O	0.2287
N_2	0.2123
O_2	0.00514
NO	0.01117
N^+	0.00276
O^+	0.00019
N_2^+	0.00204
O_2^+	0.00035
NO^+	0.00058
e^-	0.00594
Total number density	4.89×10^{16} cm^{-3}
Total radiation power through Gaussian slit	33.3 W/cm^3
Equilibration point conditions	
Location measured from shock	1.45 cm
Location measured from foot of luminosity x_e	1.09 cm
Time measured from foot of luminosity τ_e	1.09 μs
$\tau_e p_\infty$	1.49×10^{-4} μs-atm
T	13152 K
T_v	9703 K
Species mole fractions	
N	0.7316
O	0.2090
N_2	0.02935
O_2	0.00007
NO	0.00143
N^+	0.01240
O^+	0.00128
N_2^+	0.00032
O_2^+	0.00000
NO^+	0.00028
e^-	0.01420
Total number density	8.71×10^{16} cm^{-3}
Total radiation power through Gaussian slit	8.53 W/cm^3
Total radiative heat flux	7.10 W/cm^2
Nonequilibrium-to-equilibrium heat flux	2.26

3. Note that electron density rises rather slowly and that the peak radiation point is not associated with the number density of N_2^+, which is the predominant radiator in the shorter wavelength region shown in Fig. 2. As mentioned earlier, the N_2 first positive radiation peaks also at around the same point even though the two radiation mechanisms are not directly related.

The characteristic relaxation times τ_p and τ_e calculated in the present work are compared with those measured in a shock tube[13] in Fig. 4. As seen in Fig. 4, the current method reproduces the characteristic times within the scatter of the experimental data, although τ_e is slightly underestimated by the theory at $V_\infty = 6$ km/s, and overestimated at 8 km/s.

The spectra calculated at the peak intensity point are compared with the experimental spectra in Fig. 5. The calculated spectra represent the intensity values uncorrected for the instrument broadening by the slit, which is averaged over a photon energy band of 0.0269 eV. The theory significantly overestimates the spectral intensity at wavelengths between 0.3 and 0.5 μm and underestimates it at wavelengths above 0.6 μm.

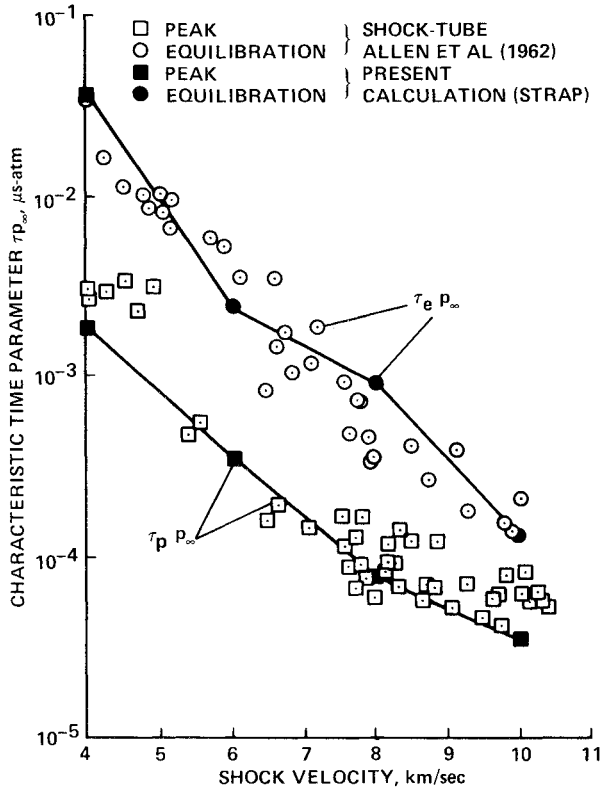

Fig. 4 Comparison between calculated and measured characteristic relaxation times of the 0.55 to 1.0 μm radiation; measurement by Allen et al.[13]

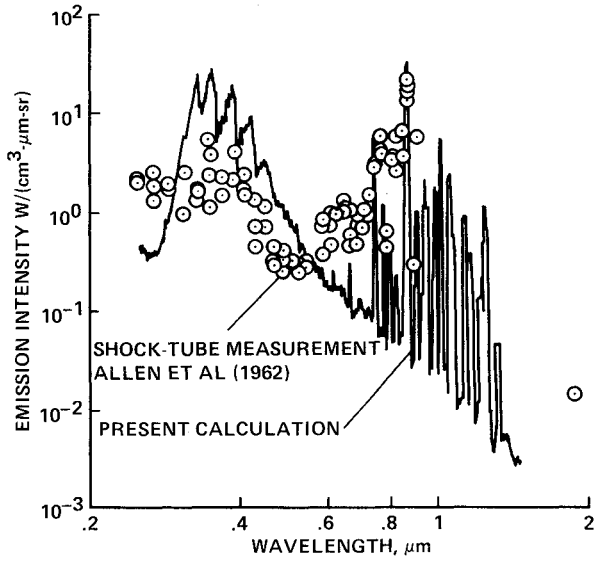

Fig. 5 Comparison between calculated and measured spectra at peak-radiation point of the 0.55 to 1.0 μm radiation; $p_\infty = 0.1$ Torr, $V_\infty =$ 10 km/s; measurement by Allen et al.[13]

The overestimate between 0.3 and 0.5 μm is caused by too high a value for the concentration of N_2^+ molecule in the $B^2\Sigma_u^+$ state, which is the upper state of the N_2^+ first negative band system. The population of this state could be overestimated because 1) the total N_2^+ concentration is too high, 2) the rotational dissociation, which is presently ignored in the calculation, is significant, and 3) the vibrational temperature of N_2^+ is too high. The total population of N_2^+ is estimated to be uncertain by a factor of about 1.5, and the rotational dissociation effect at these high temperatures might lower the population also by a similar factor.

The effect of the vibrational temperature is more complex. The vibrational temperature in the present model is assumed to be the same for all diatomic species. However, Ref. 12 contains a measurement of the vibrational temperature in the N_2^+ first negative system for a shock velocity of 6.4 km/s and freestream pressure of 1 Torr. These measurements show that the vibrational temperature of N_2^+ is lower than the vibrational temperature in the ground state ($X^2\Sigma_g^+$) of N_2 by a factor of about five at the peak intensity point (see the Introduction). The overall rate of electronic excitation of an upper electronic state is the sum over all lower and upper vibrational quantum numbers for electronic state of the rate of transition from one vibrational state in the lower electronic state to one vibrational state in the upper electronic state. The rate of collisional transition from one lower vibrational state to one higher vibrational state is, in turn, proportional to the Franck–Condon factor associated with the two vibrational states. In the case of the N_2^+ first negative system, the Franck–Condon factors are such that excitation may occur preferentially from elevated vibrational states. A lower vibrational temperature decreases the portion of the total species number density in the elevated vibrational states and, hence, lowers the overall rate of collisional electronic excitation of the B state. An estimate of this effect indicates that the concentration of the B state may be lower than the presently calculated value by a factor of 2.5–3. If these phenomena could be correctly accounted for, agreement between the theory and experiment would be closer.

The underestimate in the spectral intensity above 0.6 μm is believed to be caused primarily by not including many diffuse N- and O-atom lines that occur in this spectral region. At the high temperatures occurring in the present work, a large number of atomic levels close to the ionization limit could be significantly populated, causing the present theoretical results to be substantially low. Steps to correct for this phenomenon are also being considered. The errors in the spectral intensity just discussed do not greatly affect the integrated heat fluxes, as they are only a portion of the total flux and the two phenomena tend to offset each other.

The radiative heat flux integrated to the equilibration point q_{ne} is compared between theory and experiment in Fig. 6. The experimental data are taken from three shock-tube experiments[13,15] and two ballistic-range experiments.[16,17] As seen here, the present calculation closely reproduces all experimental points, except the upper-limit point given in Ref. 13. This point was determined in Ref. 13 by drawing a curve over the spectral plot, similar to that shown in Fig. 5, and integrating the area under it, which is an obvious overestimation of the true value. All other data are represented reasonably closely by the expression.

$$\log_{10} q_{ne} = -2.217 - 0.05V_\infty + 0.0167V_\infty^2 \quad \text{W cm}^{-2}$$

The present calculation at $V_\infty = 8$ km/s is higher than this expression because at this velocity, the present calculation overestimates the equilibration distance as shown in Fig. 4. Conversely, the present calculation at $V_\infty = 6$ km/s slightly underestimates the equilibration distance and, hence q_{ne}.

Project Fire 2 Data

The values of T, T_v, and radiation emission power calculated for the stagnation streamline of the Fire 2 vehicle are shown in Fig. 7. One case is for a freestream density of 2.21×10^{-5} and the other for 5.98×10^{-5} kg/m^3, corresponding to the altitudes of 79.13 and 73.72 km. For both cases, T_v is much smaller than T throughout the shock layer. The peak values of T_v are below 12,000 K even though T starts from 62,000 K. The thickness of the shock layer is significantly different between the two cases in that the higher-density case results in a smaller thickness. When compared with the equilibrium shock-layer thickness given in Ref. 30,

the calculated nonequilibrium shock-layer thicknesses are significantly larger.

The peak radiation occurs well away from the shock wave. In the case of $\rho_\infty = 2.21 \times 10^{-5}$, the peak radiation occurs in the inviscid region just outside of the edge of the boundary layer. The radiation is truncated in this case by the encroachment of the boundary layer. The peak intensity in the low-density case is about 40% of that of the high-density case, in rough proportion to the respective densities. The area under the intensity curves, which correspond to the wall radiative heat fluxes q_{ne}, is also roughly proportional to the densities.

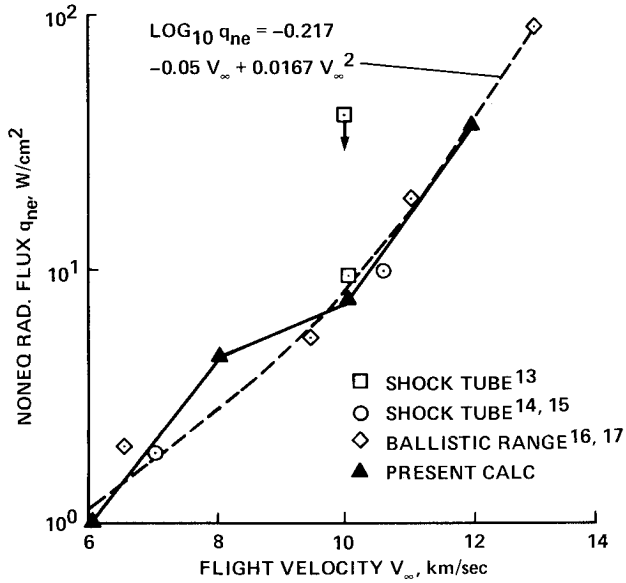

Fig. 6 Comparison between calculated and measured nonequilibrium radiative heat fluxes at the equilibration point as a function of the flight velocity.

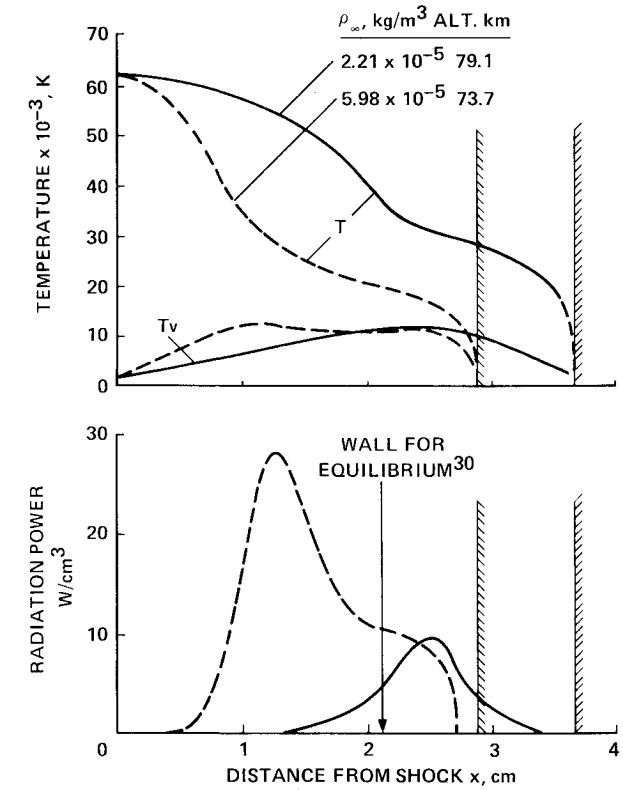

Fig. 7 Calculated temperatures and radiation emissions along the stagnation streamline in the shock layer of Fire 2 vehicle at two altitudes.

This observed feature is contrary to the concept of binary scaling of nonequilibrium radiation. The binary scaling concept assumes that the total radiation emitted by a nonequilibrium shock layer is independent of density or shock-layer thickness.[2,13]

The species mole fractions for the low-density case given in Fig. 7 are shown in Fig. 8. It is interesting to note that the

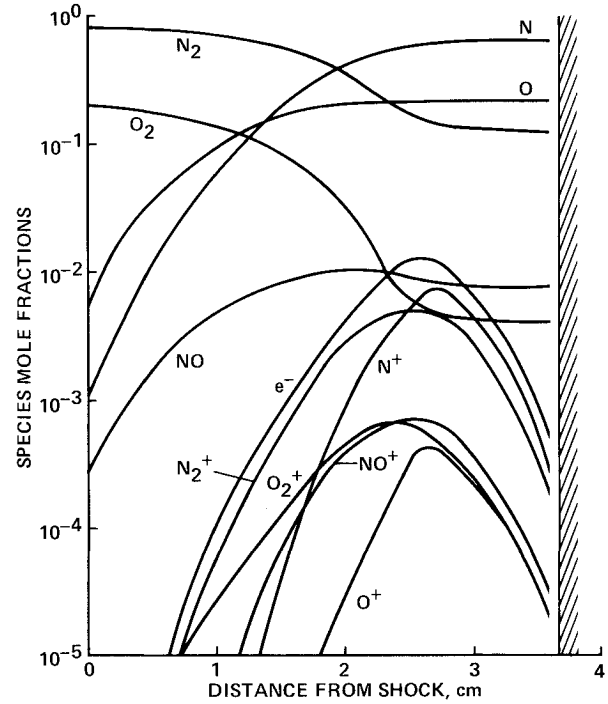

Fig. 8 Calculated species mole fractions along the stagnation streamline in the shock layer of Fire 2 vehicle at an altitude of 79.1 km, $\rho_\infty = 2.21 \times 10^{-5}$ kg/m^3, $V_\infty = 11.3$ km/s.

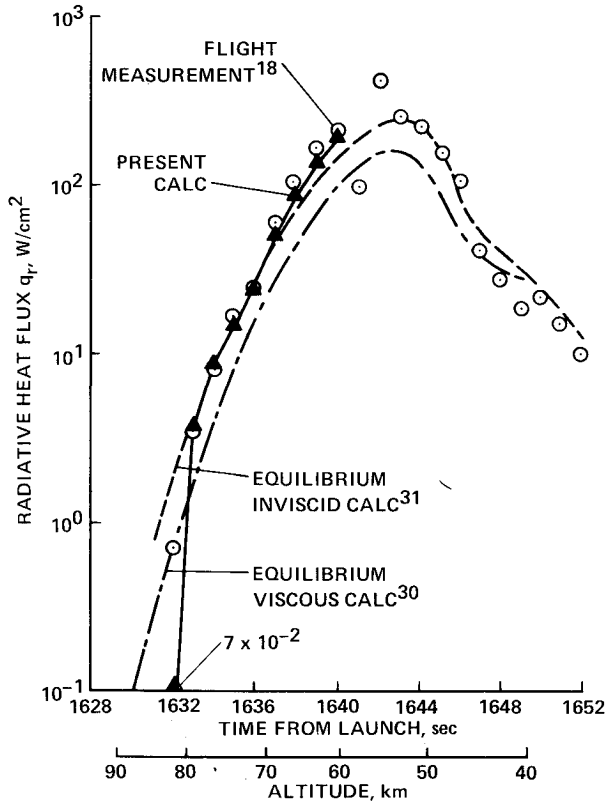

Fig. 9 Comparison between calculated and measured stagnation-point radiative heat fluxes for Fire 2 (Ref. 18).

electron mole fraction is only slightly above 1% here, as compared with the equilibrium value that would be more than 20%.

The calculated radiative heat fluxes are compared with the measured values[18] for Fire 2 in Fig. 9. The calculation is not carried out for altitudes below 60 km because the viscous-shock-layer calculation used here is inaccurate at such high-density regimes. Also shown are the equilibrium-inviscid calculation of Sutton[31] and equilibrium-viscous calculation of Balakrishnan et al.[30] The present calculation agrees closely with the measurements at altitudes below 81 km. At an altitude of 81 km, the calculation severely underestimates the heat flux. The discrepancy is most likely caused by the finite thickness of the shock wave that is neglected in the present continuum theory. The present theory assumes the shock wave to be infinitesimally thin and therefore that there is no chemical-kinetic process within the shock wave. At an altitude of 81 km, the true thickness of the shock wave becomes comparable to the thickness of the shock layer.[32] The collision processes occurring within the shock wave cause the gas molecules to be excited, or even dissociated, before they reach the continuum regime behind the shock wave. This phenomenon can be treated with a Monte Carlo technique,[32] but this was not done in this work. It is interesting to note that the equilibrium-inviscid calculation of Sutton[31] and the present nonequilibrium calculation result in virtually the same radiative heat flux values. This may be due to the compensating errors in the equilibrium theory that underestimates the intensity of radiation in the nonequilibrium regime but overestimates the thickness of the emitting layer by ignoring the boundary layer. When the boundary-layer thickness is accounted for, as in the calculation by Balakrishnan et al.,[30] the equilibrium values underestimate the measured values.

Ballistic Range Data

Calculations similar to those just discussed have been performed for small models launched in a ballistic range.[16] In these experiments, the models were made of several different types of plastics, and the tests were made at three different freestream velocities: 6.4, 9.45, and 11 km/s. Comparison is shown here for the 9.45 km/s case. For this flight velocity, two different nose radii were tested: 0.508 and 1.56 cm. In the case of 0.508 cm nose radius, the ratio of the overall radius of the model to the nose radius was sufficiently large to establish a flowfield similar to that over a spherical nose. However, for the 1.56 cm case, this ratio was too small to do so. The flowfield established over the nose region in this case resembled that over a flat disk. Over a flat disk, the shock standoff distance is nearly three times that over a sphere, and this effect must be accounted for. Unfortunately, the exact shock stand off distance is unknown at this time, and the present calculation was performed assuming an effective spherical-nose radius for the model of 1.5 times 1.56 cm.

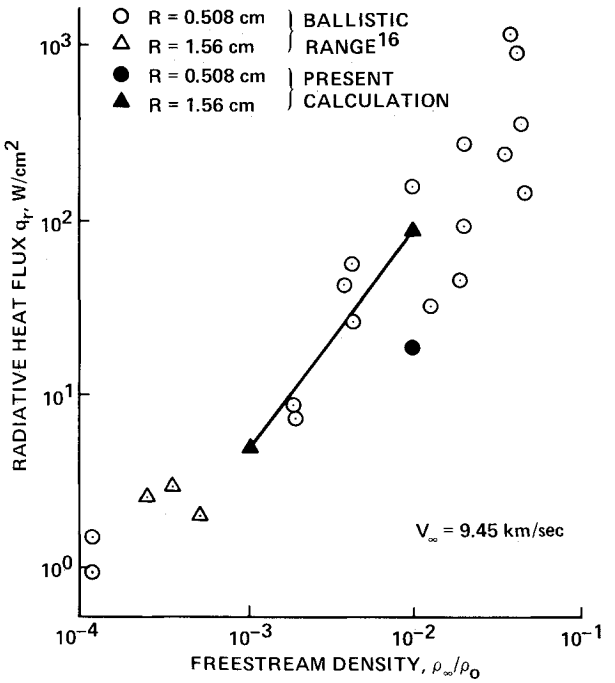

Fig. 10 Comparison between calculated and measured stagnation-point radiative heat fluxes in the ballistic-range experiment.[16]

The measured and calculated radiative heat fluxes for the ballistic-range experiment are compared in Fig. 10. As shown here, the calculated points fall within the limits of the experimental scatter. Calculation was not possible at densities below $\rho_\infty/\rho_0 = 10^{-3}$ because of the truncation phenomenon seen for the 81 km point in Fig. 9. The same truncation problem occurred for most of the 6.4 km/s cases. The case of $V_\infty =$ 11 km/s resulted in an agreement similar to that shown in Fig. 10.

At $\rho_\infty/\rho_0 = 10^{-2}$, the calculated radiative heat fluxes for the two model sizes differ substantially and are nearly proportional to the nose radii. But the experimental data show no such trend. This might be explained by the presence of ablation product species for the small nose-radius models. For these models, the convective heat-transfer rates are believed to be so high that severe ablation occurred; therefore, the shock layer contained a significant amount of ablation product species consisting of carbon compounds.[16]

Project PAET Data

In the PAET experiment, the intensity of radiation in several narrow wavelength channels was measured at the stagnation point of a spherical nose reentry body.[19,20] The data taken in the channel at 391.0 nm using a filter of 3.1 nm half-width have been analyzed in detail and reported.[20] For this channel, the filter had a spectral response such that its half-width spanned from 389.64 to 392.76 nm, and the points of 5% of peak transmission occurred at 387.6 and 395.0 nm. This wavelength range measured mainly the radiation from the $\Delta v = 0$ sequence of the first negative band system of N_2^+. However, it also admitted a portion of the $\Delta v = 0$ sequence of the violet band system of the CN molecule located just below 388.7 nm. Atmospheric air contains carbon dioxide, which produces CN behind a shock wave. The CN radiation was about an order of magnitude stronger that the N_2^+ radiation.[20] When folded with the transmission curve of the filter, the CN radiation is believed to contribute almost equally to the observed voltage rise in the detector as the N_2^+ radiation. Since the present calculation does not include CN radiation, the present comparison can be only partial. In the experiment, the background radiation was measured at 394.7 nm. The

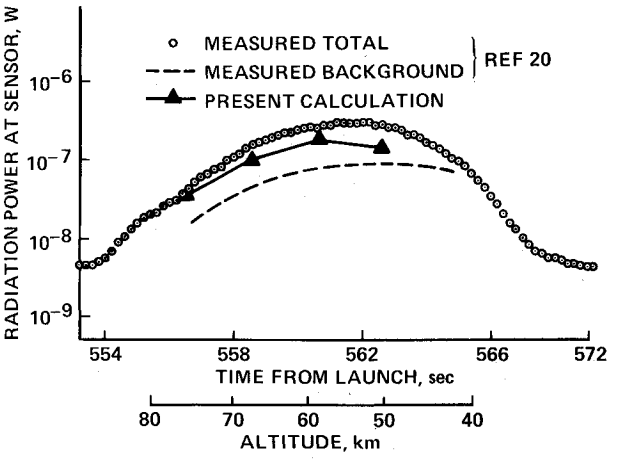

Fig. 11 Comparison between calculated and measured radiation intensities at 391 nm in PAET experiment.[20]

difference between the radiation at 391.0 and that at 394.7 nm was considered in Ref. 20 to represent the true radiation by N_2^+ and CN.

The calculated and measured radiation intensities occurring in the channel at 391.0 nm are compared in Fig. 11. The figure also shows the background radiation. The background radiation was given in Ref. 20 only up to an altitude of 67 km and is extrapolated to 74 km in the present work. As seen in the figure, the present calculation consistently underestimates the measurement. At 50 km altitude, the calculated value is only about 40% of the measured value, and this discrepancy is entirely consistent and expected due to the CN radiation that is not included in the present calculation.

Discussion

General Trend of Nonequilibrium Radiation

The preceding comparisons between the theoretical results using the present two-temperature model and the experimental data show that this model is fairly accurate in reproducing most of the experimentally obtained radiation data. The model is reasonably accurate in reproducing the relaxation times and spatially integrated radiation intensity, but is not as accurate in reproducing the observed spectra at very high temperatures. As a whole, however, one can conclude that the two-temperature kinetic model characterizes most of the principal features of nonequilibrium airflows and is much simpler than a more accurate three-temperature model.[5]

Based on the current assessment, one is encouraged to use the model to predict the radiative heat fluxes at the stagnation point of the proposed AOTV vehicle.[2] The results of such a calculation are reported here for a vehicle with a nose radius of 6 m for a gas mixture of 21% O_2 and 79% N_2 over a wide range of freestream densities and velocities. The calculated values are plotted against the product $\rho_\infty R$ in Fig. 12. The parameter $\rho_\infty R$ was chosen in recognition of the trend seen in Fig. 7 that the radiation intensity in the nonequilibrium regime is approximately proportional to the freestream density and shock-layer thickness. The figure also shows the Fire 2 values for comparison.

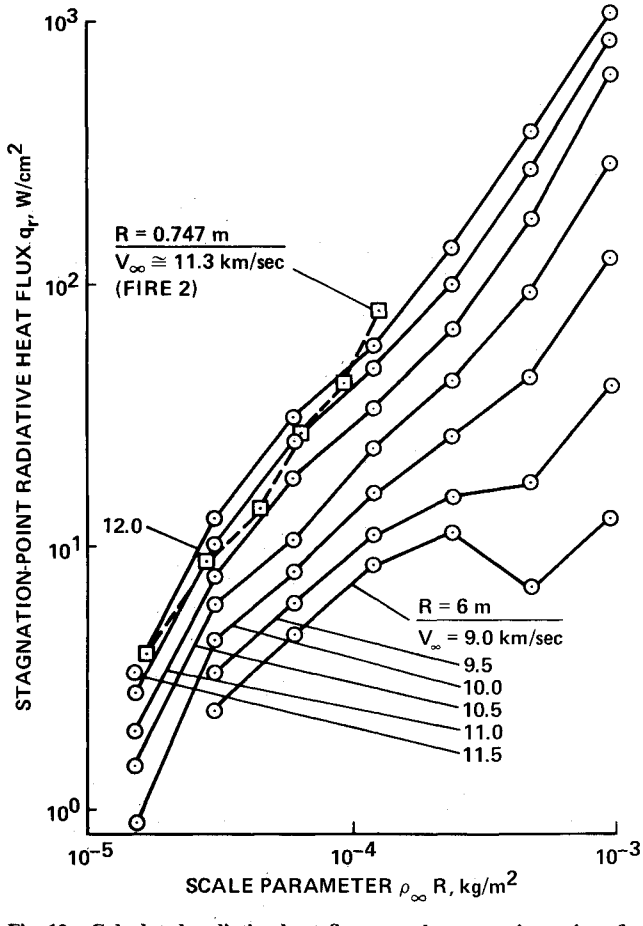

Fig. 12 Calculated radiative heat fluxes at the stagnation point of a 6 m and a 0.747 m sphere (Fire 2 vehicle) plotted against the scale parameter $\rho_\infty R$.

The calculated radiative heat flux values vary from about 1 to 1000 W/cm^2. Considering that the typical convective heat-transfer rates to the stagnation point of an entry vehicle, such as the Space Shuttle, are below 100 W/cm^2, one sees that radiative heat fluxes can be a significant portion of the total heat-transfer rate. Addition of CO_2 to the gas mixture would increase the heat-transfer rates somewhat because of the presence of the strong radiation molecule CN in the shock layer. The present heat flux values are substantially higher than those given in Ref. 29.

At the lower velocities of 9 and 9.5 km/s, Fig. 12 exhibits two linear regimes: one for $\rho_\infty R$ below 2×10^{-4} and the other above 5×10^{-4} kg/m^2. The two linear regimes are connected by a transitional region. The linear regime at the lower densities occurs in the nonequilibrium flow region. The linearity there can be attributed to the fact that the radiation intensity is approximately proportional to density, whereas the emitting volume is relatively constant (Fig. 7). The linear regime in the higher-density region occurs in the equilibrium flow region. In equilibrium flow, radiation tends to vary linearly with density, provided the radiation emanates mostly from molecules.

At flight velocities above about 10 km/s, the two linear regimes merge to form single continuous curves. Also, for these high velocities, radiative heat fluxes vary more rapidly than linear with density. This is because, for such high velocities, atomic line radiation is dominant, and the intensity of atomic line radiation is proportional approximately to the square of electron density. The electron density in turn, under equilibrium, is proportional roughly to a three-fourth power of density. As a result, radiation is proportional roughly to a one and one-half power of density in this regime. The transition from the linear relationship for nonequilibrium radiation at low densities to the equilibrium one and one-half power relationship results in the merging of the two regimes as shown.

The calculated radiative heat flux values for the Fire 2 vehicle are very similar to those for the 6 m nose-radius AOTV, even though the nose radius of the Fire 2 vehicle was only 0.747 m. This is further evidence that nonequilibrium radiative heat fluxes vary approximately linearly with the product $\rho_\infty R$. Thus, Fig. 12 is approximately universal, and the radiative heat flux for a nose radius different from 6 m can be estimated from this figure.

Limitations of the Present Kinetic Model

The current two-temperature model relies on the following assumptions:

1) Rotational temperature is the same as the translational temperature and the average energy contained in the rotational mode is kT.

2) The internal energy can be separated between the rotational, vibrational, and electronic excitation mode, with the vibrational energy approximated by kT_v.

3) There exists a limiting cross section for vibrational relaxation at high temperatures.

4) The diffusive behavior of vibrational relaxation can be represented by the sth power dependence of the vibrational relaxation rate [Eqs. (3) and (4)].

5) The dissociation rate coefficients used in the calculation implicitly account for the effect of preferential removal of high vibrational states in dissociation, and therefore, the effect needs not be accounted for explicitly.

6) The dissociation rates are dictated by the geometric average temperature $T_a = \sqrt{TT_v}$.

The first assumption is based on the experimental evidence presented in Ref. 7. However, the experimental data show a fairly large scatter. Moreover, the data are absent in the region immediately behind the shock wave where the departure of the rotational temperature from the translational temperature is most likely to occur. It is possible that the rotational temperature is different from the translational temperature in the high-temperature regime considered in the present work, especially in the region immediately behind the shock wave. Also, when rotational temperature exceeds 30,000 K, as is the case in most of the examples considered in the present work, the truncation of the rotational levels (finiteness of the allowed rotational levels) renders the energy content in the rotational mode to be substantially less than kT (Ref. 33). This truncation phenomenon and the disequilibrium between the two temperatures invalidate the concept of the common translational-rotational temperature. The translational-rotational temperature T used in the present work must be interpreted as an average temperature between the two temperatures, so that $2.5\,kT$ represents the sum of the energies contained in the two modes.

The second assumption of separable internal energies has been shown to be valid approximately for temperatures below about 10,000 K (Ref. 33). The vibrational energy expression of kT_v used in the present work is approximately valid also below about 10,000 K (but higher than about 7000 K) for N_2, which is the main vibrator in the present regime of interest. Vibrational, and hence the electronic excitation, temperature remained between 7000 and 12,000 K in the region emitting radiation. Hence, provided the rotational energy is defined as given here, the present treatment of vibrational and electronic modes should be valid approximately.

The rest of the assumptions are novel and unique to the present model. The reasons for the third and fifth assumptions have been given in Ref. 7 and the earlier parts of the present paper. Assumption six is arbitrary, but is not without grounds. In the past, efforts have been made to theoretically derive the expression for the rate coefficients from the first principles.[34,35] In Ref. 34, in a formulation known as the CVD model, the rate expression is derived for a rotationless harmonic oscillator for the case where the vibrational levels are populated according to the Boltzmann distribution. For the range of conditions of present interest, the CVD rate coefficient can be reproduced approximately by a variation of the present model in which the average temperature is defined as

$$T_a = T^q T_v^{1-q}, \qquad q = 0.7 \tag{5}$$

Calculations have been carried out using this average temperature for the Fire 2 case. The results were found to overpredict radiation considerably, indicating that the $q = 0.7$ value underestimates the influence of vibrational temperature. One may surmise that the present model ($q = 0.5$) implicitly contains the effect of the nonequilibrium rotational temperature: If rotational temperature T_r is different from the translational temperature T, then its effect on the reaction rate coefficient could be represented approximately by an average temperature of the form

$$T_a = T^q T_r^r T_v^{1-q-r} \tag{6}$$

If $q = 0.5$, $r = 0.2$, and $T_r = T$, then Eq. (6) becomes approximately equal to the CVD model. If $q = 0.5$, $r = 0.2$, and $T_r = T_v$, Eq. (6) becomes identical to the present model. The CVD model is likely to be in error also in the assumption of the Boltzmann distribution of the vibrational levels. Reference 35 extended the CVD model to include rotational motion, but still assumed Boltzmann distribution.

In addition to the uncertainties about the model used, there are additional uncertainties due to the lack of information. For instance, the vibrational relaxation times have been calculated in the present work using the correlation formula of Millikan and White.[23] Existing experimental data[36] show that the vibrational relaxation time of O_2 in collision with O is orders of magnitude shorter than that calculated using the formula. The relaxation time for N_2 in collision with O, which is the most important vibrational rate parameter in the present problem but is unknown, is likely to behave in a similar manner. Also, the exchange reactions such as $N_2 + O \rightarrow NO + O$ are assumed to be controlled by T alone. This reaction could be affected by the vibrational temperature. Also, the reaction rate coefficients have been extrapolated from the existing data taken at temperatures typically below 10,000 K to much higher temperatures. Several rate coefficients are unknown and have been arbitrarily assumed (see the appendix).

Because of the large multiplicity of the parameters, it is senseless to attempt to conduct a systematic sensitivity study. However, a limited sensitivity study has been carried out in the present work. The study shows that the calculated radiation intensity and characteristic times are most sensitive, roughly in order of importance, to 1) the choice of q in Eq. (5), 2) the choice of s in Eq. (3), 3) the choice of σ_v in the expression for τ_c [Eqs. (1) and (2)], 4) the choice of the vibrational relaxation times for N_2 and O_2 in collision with O, 5) the choice of the rate coefficient for the $N_2 + e \rightarrow N + N + e$, and 6) the choice of the temperature dependence [$q = 0.5$ or 1 in Eq. (5)] for the exchange reactions $NO + O \rightarrow N + O_2$ and $N_2 + O \rightarrow NO + O$.

The reaction $N_2 + e \rightarrow N + N + e$ almost solely determines the equilibration distance in the present regime of interest. Its rate has never been measured and is estimated from the results given in Ref. 7. The two neutral NO exchange reactions determine the rate of formation of N, which in turn determines the rate of formation of N_2^+ through the reaction $N + N \rightarrow N_2^+ + e$. The calculated radiation characteristics are fairly insensitive to the choice of rate constants for the remaining reactions. For those reactions for which the rate coefficients have been measured by more than one investigator, any of those measured values lead to approximately the same results. Thus, except for the $N_2 + e \rightarrow N + N + e$, all uncertainties concern the thermal nonequilibrium phenomena for which there are no reliable theoretical or experimental data at present. A large change in any reaction rate coefficient can be compensated for by a small change in q, s, or σ_v.

Conclusions

The present two-temperature model assumes that one temperature T characterizes the heavy-particle translational and molecular rotational energies, and another temperature T_v characterizes the molecular vibrational, electron translational, and electronic excitation energies and accounts for the limiting cross section and diffusive nature of vibrational relaxation at high temperatures. Substantial agreement is seen between the theoretical and experimental results obtained in shock tubes, ballistic ranges, and flight experiments for relaxation times and radiative heat fluxes. The spectral calculations need further improvement. The agreement provides strong evidence that the model characterizes the principal features of nonequilibrium airflows. New theoretical results using the model are presented for the radiative heat fluxes at the stagnation point of a 6 m radius sphere, representing an AOTV, over a range of freestream conditions. Problems remain in verifying the underlying assumptions individually.

Appendix: Reaction Rate Coefficients

The preexponential factor C and temperature exponent n in the rate coefficients for dissociation of O_2 by collisions with O_2 given in Table 1 are the best-fit values obtained in the present work to the experimental data of Mathews,[37] Byron,[38] Schexnayder and Evans,[39] Generalov and Losev,[40] Rink et

al.,[41] and Camac and Vaughn.[42] Those for collisions with O are the best-fit values obtained also in the present work to the data of Byron,[38] Rink et al.[41] and Camac and Vaughn.[42] The values for collisions with N_2 and NO are assumed to be the same as those for collisions with O_2. The values for the case of the collisions with N and e^- are assumed to be the same as for collisions with O, except for the case of N_2 dissociating by the impact of e^- mentioned earlier.

The rate parameters for dissociation of N_2 by the collisions of N_2 and N are from the work of Appleton et al.[43] The rate coefficient for the collisions with O is assumed arbitrarily to be three times that for collisions with N. The rate coefficient for collisions with O_2 is assumed to be the same as for collisions with N_2. The rate coefficient for collisions with NO chosen, shown in Table 1, is also arbitrary.

The rate coefficient for dissociation of N_2 by the collisions of e^- is taken from Ref. 7, in which it is deduced from the rate of final equilibration at large times.

The rate parameters for dissociation of NO are the best-fit values obtained in the present work to the data presented in the work of Baulch et al.[44]

The rate coefficient for the two exchange reactions $NO + O \rightarrow N + O_2$ and $O + N_2 \rightarrow N + NO$ are obtained from Refs. 45 and 46. All charge exchange reactions are estimated as in Ref. 47. The rate parameters for the three associative ionization rates $N + O \rightarrow NO^+ + e^-$, $O + O \rightarrow O_2^+ + e^-$, and $N + N \rightarrow N_2^+ + e^-$ are deduced from Refs. 48 to 50. (The values are different from those in Ref. 6 by a factor of 100. This difference is attributed to a typographical error in Ref. 6.)

The electron-impact ionization rate coefficient for $N + e^- \rightarrow N^+ + e^- + e^-$ is taken from Ref. 51. The coefficient for $O + e^- \rightarrow O^+ + e^- + e^-$ is deduced from the $N + e^-$ rate if we assume that the reverse (recombination) rates for the two reactions are the same.

References

[1]Park, C., "Radiation Enhancement by Nonequilibrium in Earth's Atmosphere," *Journal of Spacecraft and Rockets*, Vol. 22, Jan.–Feb. 1985, pp. 27–36.

[2]Park, C., "Problem of Rate Chemistry in the Flight Regimes of Aeroassisted Orbital Transfer Vehicles," *Progress in Astronautics and Aeronautics: Thermal Design of Aeroassisted Orbital Transfer Vehicles*, Vol. 96, edited by H. F. Nelson, AIAA, New York, 1985, pp. 511–537.

[3]Gnoffo, P. A., "Three-Dimensional AOTV Flowfields in Chemical Nonequilibrium," AIAA Paper 86-0230, Jan. 1986.

[4]Li, C. P., "Implicit Methods for Computing Chemically Reacting Flows," NASA TM 58274, Sept. 1986.

[5]Lee, J. H., "Basic Governing Equations for the Flight Regimes of Aeroassisted Orbital Transfer Vehicles," *Progress in Astronautics and Aeronautics: Thermal Design of Aeroassisted Orbital Transfer Vehicles*, Vol. 96, edited by H. F. Nelson, AIAA, New York, 1985, pp. 3–53.

[6]Park, C., "Convergence of Computation of Chemically Reacting Flows," *Progress in Astronautics and Aeronautics: Thermophysical Aspects of Re-Entry Flows*, Vol. 103, edited by J. N. Moss and C. D. Scott, AIAA, New York, 1986, pp. 478–513.

[7]Park, C., "Assessment of Two-Temperature Kinetic Model for Dissociating and Weakly-Ionizing Nitrogen," *Journal of Thermophysics and Heat Transfer*, Vol. 2, Jan. 1988, pp. 8–16.

[8]Park, C., "Calculation of Nonequilibrium Radiation in the Flight Regimes of Aeroassisted Orbital Transfer Vehicles," *Progress in Astronautics and Aeronautics: Thermal Design of Aeroassisted Orbital Transfer Vehicles*, Vol. 96, edited by H. F. Nelson, AIAA, New York, 1985, pp. 395–418.

[9]Park, C., "Nonequilibrium Air Radiation (NEQAIR) Program: User's Manual," NASA TM 86707, July 1985.

[10]Allen, R. A., Camm, J. C., and Keck, J. C., "Radiation from Hot Nitrogen," Avco-Everett Res. Lab., Everett, MA, Res. Rept. 102, April 1961.

[11]Allen, R. A., Keck, J. C., and Camm, J. C., "Nonequilibrium Radiation from Shock Heated Nitrogen and a Determination of the Recombination Rate," Avco-Everett Res. Lab., Everett, MA, Rept. 110, June 1961.

[12]Allen, R. A., "Nonequilibrium Shock Front Rotational, Vibrational, and Electronic Temperature Measurements," Avco-Everett Res. Lab., Everett, MA, Res. Rept. 186, Aug. 1964.

[13]Allen, R. A., Rose, P. H., and Camm, J. C., "Nonequilibrium and Equilibrium Radiation at Super-Satellite Entry Velocities," Avco-Everett Res. Lab., Everett, MA, Res. Rept. 156, Sept. 1962.

[14]Camm, J. C., Kivel, B., Taylor, R. L., and Teare, J. D., "Absolute Intensity of Nonequilibrium Radiation in Air and Stagnation Heating at High Altitudes," Avco-Everett Res. Lab., Everett, MA, Res. Rept. 93, Dec. 1959.

[15]Teare, J. D., Georgiev, S., and Allen, R. A., "Radiation from the Nonequilibrium Shock Front," Avco-Everett Res. Lab., Everett, MA, Res. Rept. 112, Oct. 1961.

[16]Page, W. A. and Arnold, J. O., "Shock-Layer Radiation of Blunt Bodies at Reentry Velocities," NASA TR R-193, April 1964.

[17]Canning, T. N. and Page, W. A., "Measurements of Radiation from the Flow Fields of Bodies Flying at Speeds Up to 13.4 Kilometers per Second," Presented to fluid mechanics panel of AGARD, Brussels, Belgium, April 1962.

[18]Cauchon, D. L., "Radiative Heating Results from the Fire 2 Flight Experiment in a Reentry Velocity of 11.3 Kilometers per Second," NASA TM X-1402, 1967.

[19]Seiff, A., Reese, D. E., Sommer, S. C., Kirk, D. B., Whiting, E. E., and Niemann, H. B., "PAET, An Entry Probe Experiment in the Earth's Atmosphere," *Icarus*, Vol. 18, April 1973, pp. 525–563.

[20]Whiting, E. E., Arnold, J. O., Page, W. A., and Reynolds, R. M., "Composition of the Earth's Atmosphere by Shock-Layer Radiometry During the PAET Entry Probe Experiment," *Journal of Quantitative Spectroscopy and Radiative Transfer*, Vol. 9, Sept. 1973, pp. 837–859.

[21]Lee, J. H., "Electron-Impact Vibrational Excitation Rates in the Flowfield of Aeroassisted Orbital Transfer Vehicles," *Progress in Astronautics and Aeronautics: Thermophysical Aspects of Re-Entry Flows*, Vol. 103, edited by J. N. Moss and C. D. Scott, AIAA, New York, 1986, pp. 197–224.

[22]Treanor, C. E. and Marrone, P. V., "The Effect of Dissociation on the Rate of Vibrational Relaxation," Cornell Aeronautical Lab., Buffalo, NY, Rept. 253-62, Feb. 1962.

[23]Millikan, R. C. and White, D. R., "Systematics of Vibrational Relaxation," *Journal of Chemical Physics*, Vol. 39, Dec. 1963, pp. 3209–3213.

[24]Keck, J. C. and Carrier, G., "Diffusion Theory of Nonequilibrium Dissociation and Recombination," *Journal of Chemical Physics*, Vol. 43, July 1965, pp. 2284–2298.

[25]Yos, J. M., "Transport Properties of Nitrogen, Hydrogen, Oxygen, and Air to 30,000 K," Avco Corp., Wilmington, MA, RAD TM-63-7, 1963.

[26]Lensch, G. and Gronig, H., "Experimental Determination of Rotational Relaxation in Molecular Hydrogen and Deuterium," *Shock Tube and Shock Wave Research: Proceedings of the 11th International Symposium on Shock Tubes and Waves*, edited by B. Ahlborn, A. Hertzberg, and D. Russell, Univ. of Washington Press, Seattle, WA, 1978, pp. 132–139.

[27]Whiting, E. E., Arnold, J. O., and Lyle, G. C., "A Computer Program for a Line-by-Line Calculation of Spectra from Diatomic Molecules and Atoms Assuming a Voigt Line Profile," NASA TN D-5088, March 1969.

[28]Park, C., "Dissociative Relaxation in Viscous Hypersonic Shock Layers," *AIAA Journal*, Vol. 2, July 1964, pp. 1202–1207.

[29]Davies, C. B. and Park, C., "Aerodynamic and Thermal Characteristics of Modified Raked-Off Blunted Cones," AIAA Paper 86-1309, June 1986.

[30]Balakrishnan, A., Park, C., and Green, M. J., "Radiative Viscous Shock Layer Analysis of Fire, Apollo, and PAET Flight Data," *Progress in Astronautics and Aeronautics: Thermophysical Aspects of Re-Entry Flows*, Vol. 103, edited by J. N. Moss and C. D. Scott, AIAA, New York, 1986, pp. 514–540.

[31]Sutton, K., "Air Radiation Revisited," *Progress in Astronautics and Aeronautics: Thermal Design of Aeroassisted Orbital Transfer Vehicles*, Vol. 96, edited by H. F. Nelson, AIAA, New York, 1985, pp. 419–441.

[32]Moss, J. N., Cuda, V., and Simmonds, A. L., "Nonequilibrium Effects for Hypersonic Transitional Flows," AIAA Paper 87-0404, Jan. 1987.

[33]Jaffe, R. L., "The Calculation of High-Temperature Equilibrium and Nonequilibrium Specific Heat Data for N_2, O_2, and NO," AIAA Paper 87-1633, June 1987.

[34]Hammerling, P., Teare, J. D., and Kivel, B., "Theory of Radiation from Luminous Shock Waves in Nitrogen," *Physics of Fluids*, Vol. 2, July–Aug. 1959, pp. 422–426.

[35]Jaffe, R. L., "Rate Constants for Chemical Reactions in High Temperature Nonequilibrium Air," *Progress in Astronautics and Aeronautics: Thermophysical Aspects of Re-Entry Flows*, Vol. 103, edited by J. N. Moss and C. D. Scott, AIAA, New York, 1986, pp. 123–151.

[36]Kiefer, J. H. and Lutz, R. W., "The Effect of Oxygen Atoms on the Vibrational Relaxation of Oxygen," *Proceedings of the 11th Symposium (International) on Combustion*, The Combustion Inst., Pittsburgh, PA, 1967, pp. 67–76.

[37]Mathews, S. L., "Interferometric Measurement in the Shock Tube of the Dissociation Rate of Oxygen," *Physics of Fluids*, Vol. 2, March–April 1959, pp. 170–178.

[38]Byron, S. R., "Measurement of the Rate of Dissociation of Oxygen," *Journal of Chemical Physics*, Vol. 30, June 1959, pp. 1380–1392.

[39]Schexnayder, C. J. and Evans, J. S., "Measurement of the Dissociation Rate of Molecular Oxygen," NASA TR R-108, 1961.

[40]Generalov, N. A. and Losev, S. A., "Vibrational Excitation and Molecular Dissociation of Gaseous Oxygen and Carbon Dioxide in a Shock Wave," *Journal of Quantitative Spectroscopy and Radiative Transfer*, Vol. 6, Jan.–Feb. 1966, pp. 101–125.

[41]Rink, J. P., Knight, H. T., and Duff, R. E., "Shock Tube Determination of Dissociation Rates of Oxygen," *Journal of Chemical Physics*, Vol. 34, June 1961, pp. 1942–1947.

[42]Camac, M., and Vaughn, A., "O_2 Dissociation Rates in O_2-A, Mixtures," *Journal of Chemical Physics*, Vol. 34, Feb. 1961, pp. 460–470.

[43]Appleton, J. P., Steinberg, M., and Liquornik, D. J., "Shock-Tube Study of Nitrogen Dissociation Using Vacuum-Ultraviolet Light Absorption," *Journal of Chemical Physics*, Vol. 48, Jan. 1968, pp. 599–608.

[44]Baulch, D. L., Drysdale, D. D., and Horne, D. G., "Evaluated Kinetic Data for High Temperature Reactions," *Homogeneous Gas Phase Reactions of the H_2-N_2-O_2 System*, Vol. 2, CRC Press, Cleveland, OH, 1973.

[45]Hanson, R. K., Flower, W. L., and Kruger, C. H., "Determination of the Rate Constant for the Reaction $O + NO \rightarrow N + O_2$," *Combustion Science and Technology*, Vol. 9, Nos. 3 and 4, June 1974, pp. 79–86.

[46]Monat, J. P., Hanson, R. K., and Kruger, C. H., "Shock Tube Determination of the Rate Coefficient for the Reaction $N_2 + O \rightarrow NO + N$," *Proceedings of the 17th Symposium (International) on Combustion*, The Combustion Inst., Pittsburgh, PA, 1978, pp. 543–552.

[47]Bortner, M. H., "A Review of Rate Constants of Selected Reactions of Interest in Re-Entry Flow Fields in the Atmosphere," National Bureau of Standards, Washington, DC, NBS TN 484, May 1969.

[48]Dunn, M. G. and Lordi, J. A., "Measurement of Electron Temperature and Number Density in Shock Tunnel Flows, Part 2. $NO^+ + e$ Dissociative Recombination Rate in Air," *AIAA Journal*, Vol. 7, Nov. 1969, pp. 2099–2104.

[49]Dunn, M. G. and Lordi, J. A., "Measurement of $O_2^+ + e$ Dissociative Recombination in Expanding Oxygen Flows," *AIAA Journal*, Vol. 8, April 1970, pp. 614–618.

[50]Dunn, M. G. and Lordi, J. A., "Measurement of $N_2^+ + e$ Dissociative Recombination in Expanding Nitrogen Flows," *AIAA Journal*, Vol. 8, Feb. 1970, pp. 339–345.

[51]Park, C., "Measurement of Ionic Recombination Rate of Nitrogen," *AIAA Journal*, Vol. 6, Nov. 1968, pp. 2090–2094.

NEW! *from the AIAA*
Progress in Astronautics and Aeronautics Series . . .

Gun Propulsion Technology

Ludwig Stiefel, editor

Ancillary to the science of the interior ballistics of guns is a technology which is critical to the development of effective gun systems. This volume presents, for the first time, a systematic, comprehensive and up-to-date treatment of this critical technology closely associated with the launching of projectiles from guns but not commonly included in treatments of gun interior ballistics. The book is organized into broad subject areas such as ignition systems, barrel erosion and wear, muzzle phenomena, propellant thermodynamics, and novel, unconventional gun propulsion concepts. It should prove valuable both to those entering the field and to the experienced practitioners in R&D of gun-type launchers.

TO ORDER: Write AIAA Order Department,
370 L'Enfant Promenade, S.W., Washington, DC 20024
Please include postage and handling fee of $4.50 with all orders. California and D.C. residents must add 6% sales tax. All orders under $50.00 must be prepaid. All foreign orders must be prepaid. Allow 4–6 weeks for delivery.

1988 340 pp., illus. Hardback
ISBN 0-930403-20-7
AIAA Members $49.95
Nonmembers $79.95
Order Number V-109